Retrospective Correction of Angular Gain by Virtual Carouseling in MEMS Gyroscopes

Sina Askari, Mohammad H. Asadian and Andrei M. Shkel
MicroSystems Laboratory, University of California, Irvine, CA, USA
Email: {*sina.askari*, *asadianm*, *andrei.shkel*} @uci.edu

***Abstract*— We present a correction approach of angular gain based on frequency mismatch of a gyroscope operating in the Whole Angle (WA) mode. The virtual carouseling (VC) and closed-loop WA modes of operation were implemented on a Quad Mass Gyroscope (QMG). The variations in the frequency mismatch associated with the temperature drift were made observable through VC and compensated in the angular gain estimation.**

I. Introduction

A high quality factor (Q-factor) MEMS gyroscope operating in the closed-loop Whole Angle (WA) mode was developed to measure the angle of rotation directly, without the need for numerical integration of the angular rate measurements [1]. The uncompensated frequency mismatch Δf and anisodamping $\Delta(1/\tau)$ are the two major sources of drift, limiting the minimum detectable rate in the WA mode of operation [2], [3]. A Force-to-Rebalance (FTR) closed-loop is often implemented to modulate a virtual rotation by carouseling the orientation of the drive axis using the X-Y electrodes of the gyro to observe imperfections, such as frequency, damping, and gain mismatches [4]–[8].

In an ideal gyroscope operating in the WA mode, with damping and stiffness isotropy, the angular gain of precession is a function of geometry of the resonant masses. The angular gain is a coefficient translating the precession pattern of the sensing element to the angle of measured rotation of the object, and therefore is a key parameter in characterization of performance of WA gyros [9]. Fabrication imperfections break the symmetry of the gyro, thus making it susceptible to environmental disturbances, like temperature fluctuations. For example, the residual of the frequency mismatch was observed to be sensitive to temperature fluctuations [10].

In this paper, the temperature sensitivity of frequency mismatch Δf on the angular gain drift in an electrostatically tuned MEMS gyro was identified, and the correlation between the drift in the WA angular gain and temperature fluctuation was interpreted. Fig. 1 shows schematics of the correction procedure studied in this paper. The error identification and WA modes were switched for estimation and correction of the angular gain with interruption of the gyroscope operation. The extracted Δf value was used in a feed-forward manner to correct for the angular gain drift.

This material is based on work supported by the Defense Advanced Research Projects Agency under Grant N66001-16-1-4021.

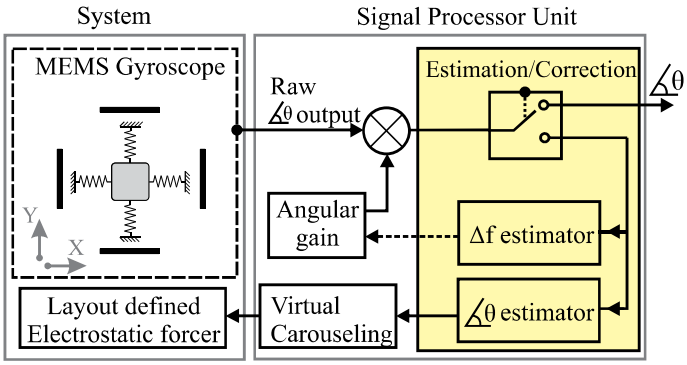

Fig. 1. Schematics of the proposed error identification technique in the whole angle mode of operation of a MEMS gyroscope.

II. Identification of error through Virtual Carouseling

The focus of this work is entirely on identification of device error parameters without physical rotation using an electrostatically emulated virtual rotation. The effectiveness of the approach was validated by a physical input rotation stimulus provided by a rate table. Virtual Carouseling (VC) allows for self-test and self-identification functionalities without relying on any external physical stimuli to the device. The block diagram of the implemented algorithm is shown in Fig. 2, with a full representation of the closed loop angle estimation and VC controls used in this study. In carouseling, a frequency mismatch, damping mismatch, and the gain errors were made observable. The measured angle of precession θ was estimated from the rate signal output at every incremental precession ($\Delta\theta$), and it was used as the direct output angle of measurement and also as an input to the system to sustain the line of oscillation (an analogy of a standing wave in continues systems). The angular gain (AG) was estimated from the precession angle of the gyro subjected to a known continuous external rotation. In the WA mode, the input changes of θ are controlled by a rate table, whereas in a VC operation the precession is controlled by a forcing function supplied to the device simulating the Coriolis force.

The trajectory of a standing wave pattern at any given angle θ can be described by an in-phase ($I(t)$) and in-quadrature ($Q(t)$) components of the oscillation frequency ω, which is in the rotating frame can be expressed as $I(t) = cos(\omega t + \phi_0)$ and $Q(t) = sin(\omega t + \phi_0)$.

The control command signals, $F_{x(t)}$ and $F_{y(t)}$, required to

978-1-5386-7828-2/19/$31.00 ©2019 IEEE

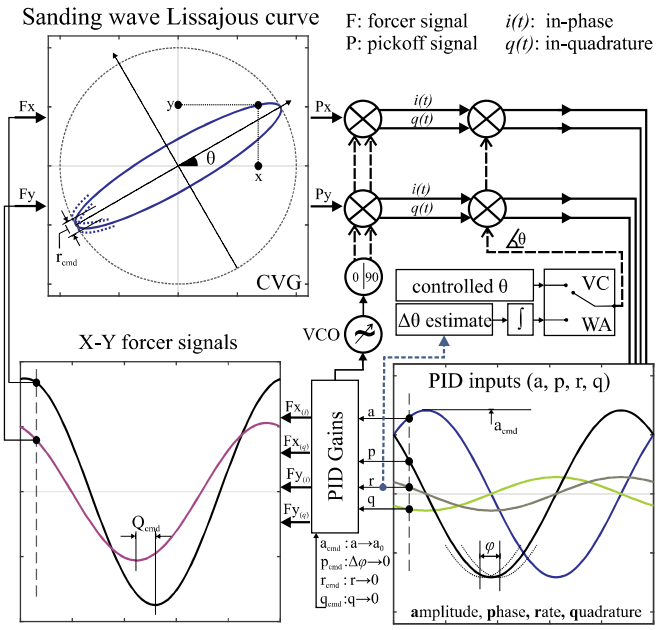

Fig. 2. Graphical representation of the implemented control loops for the WA mode of operation or VC control. The input to the PID controllers and forcer signals to the device is shown for one full wave cycle of the oscillation.

sustain such a pattern with PID set values of amplitude (a), quadrature (q), and rate (r) are expressed in terms of in-phase (i) and in-quadrature (q) components as follows [2]:

$$\mathrm{F}_{x_i(t)} = a_{cmd} \cdot Q(t) \cdot cos\theta - (q_{cmd} \cdot I(t) + r_{cmd} \cdot Q(t))\ sin\theta$$
$$\mathrm{F}_{x_q(t)} = a_{cmd} \cdot I(t) \cdot cos\theta + (q_{cmd} \cdot Q(t) - r_{cmd} \cdot I(t))\ sin\theta$$
$$\mathrm{F}_{y_i(t)} = a_{cmd} \cdot Q(t) \cdot sin\theta + (q_{cmd} \cdot I(t) + r_{cmd} \cdot Q(t))\ cos\theta$$
$$\mathrm{F}_{y_q(t)} = a_{cmd} \cdot I(t) \cdot sin\theta - (q_{cmd} \cdot Q(t) - r_{cmd} \cdot I(t))\ cos\theta$$

where index cmd represents the output of the PID controller and indexes x and y denote the X-axis and Y-axis of the device defined by the layout (intended x- and y- axes of the device), respectively. The main loops are phase-locked loop (PLL), amplitude, quadrature, and rate controls. The discrete-time control sequence input at time k for each PID controller with filters can be expressed by U(k) as follow:

$$\mathrm{U}(k)_a = +x(k)_i \cdot cos\theta + y(k)_i \cdot sin\theta$$
$$\mathrm{U}(k)_r = -x(k)_i \cdot sin\theta + y(k)_i \cdot cos\theta$$
$$\mathrm{U}(k)_p = +x(k)_q \cdot cos\theta + y(k)_q \cdot sin\theta$$
$$\mathrm{U}(k)_q = -x(k)_q \cdot sin\theta + y(k)_q \cdot cos\theta$$

After the PID loops are established, the gyro is capable of operating in the Rate, FTR, or WA modes. In the WA case, the FTR control in the rate loop is turned-off. In all of the operational modes, a Voltage-Controlled Oscillator (VCO) tracked the oscillation frequency, the quadrature command nulled the quadrature signal, and the rate command was used to estimate $\Delta\theta$.

A vacuum sealed device with a Q-factor of over 2 million and as-fabricated frequency mismatch of 15Hz was electrostatically tuned down to 220mHz and was used for virtual carouseling and estimation of the angular gain. The decay time of the "standing wave" was extracted with 12° increments, Fig. 3. The damping mismatch $\Delta(1/\tau)$ for the device under test was estimated as 1.2×10^{-4} Hz. Therefore, the damping mismatch was identified as a negligible factor for our subsequent experiments, while the frequency mismatch was identified as the major contributing source of error in the angle estimation.

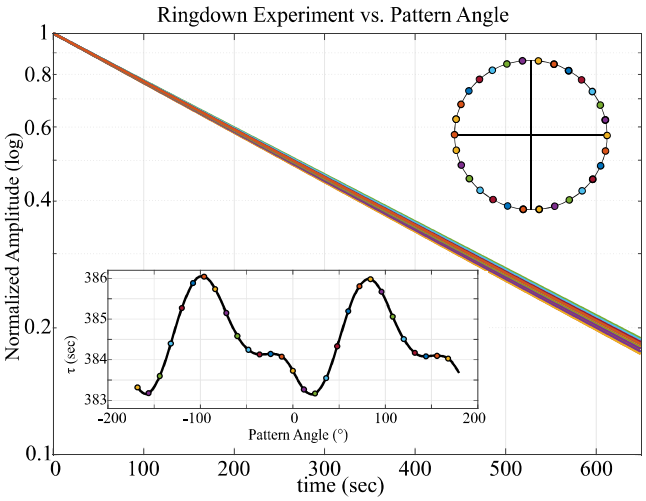

Fig. 3. Identification of $\Delta(1/\tau)$ under tuned condition at each angle by disengaging the amplitude control loop while other control loops, such as phase, quadrature, and rate, were still engaged.

Fig. 4 shows the dependency of control loop signals as a function of pattern angle. The variation in frequency and gain mismatches originated from uncompensated structural asymmetry and the gain mismatch of the electronics.

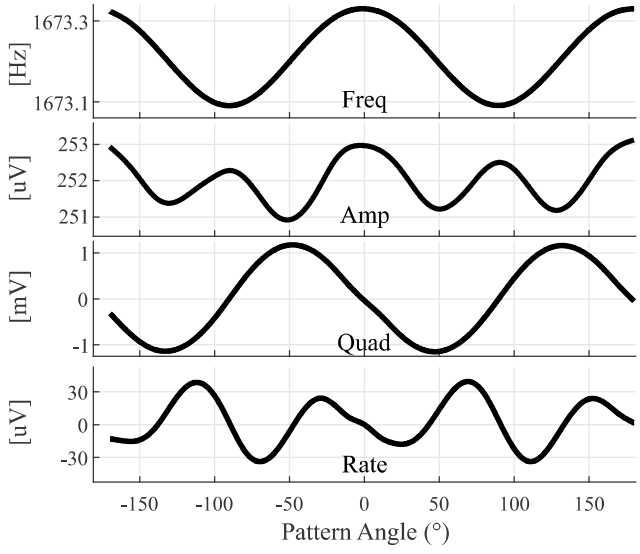

Fig. 4. Experimental error identification using virtual carouseling of the vibration pattern in response to electrostatic force rotation. The frequency mismatch and the orientation of principle axis of elasticity were observed from the PLL frequency, amplitude, quadrature, and rate command signals, showing 2θ and 4θ dependency on the pattern angle.

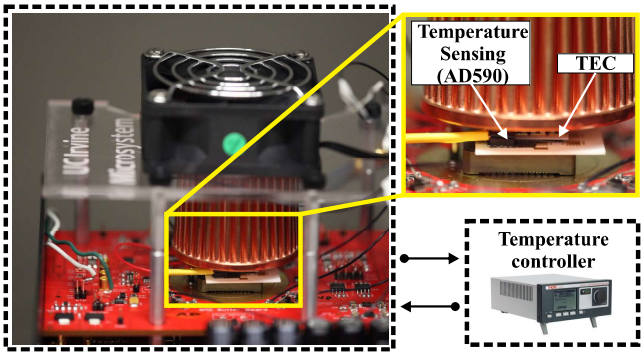

Fig. 5. Experimental setup of the localized close-loop controlled cooling/heating for the vacuum sealed device in LCC package.

III. Temperature Induced Drift

A closed-loop controlled thermal stage was developed for ovenization of the gyro in an LCC package as well as a direct recording of temperature fluctuations during the experiments, Fig. 5. The stage was composed of a temperature controller, a thermoelectric cooler (TEC), and a thermistor, with a temperature range from 20°C to 85°C. The events of temperature variations were recorded during the experiments. The temperature of the LCC package slowly rose up to about 32°C as a result of electronics power-up (Fig. 6a). As the rate table rotation started, the temperature dropped by 1°C due to convective cooling of the rate table (Fig. 6b). Fig. 6c illustrates the closed-loop ovenization and stability of temperature for the calibration purpose, demonstrating stability of temperature fluctuations within 0.04 °C.

Fig. 7 shows frequency mismatch variations at different temperatures through virtual carouseling. At every temperature, the frequency mismatch was estimated from a range of frequency parameters extracted experimentally as a maximum deviation in peak-to-peak values. The results show 160mHz

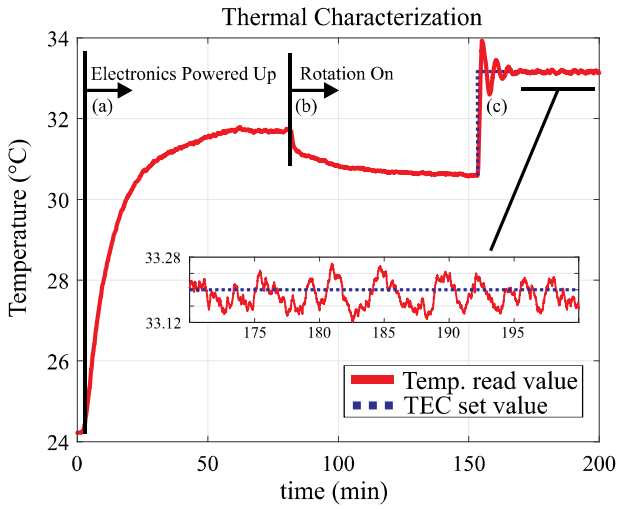

Fig. 6. Illustration of temperature events for one complete characterization cycle from room temperature: a) front-end electronics powered up, b) start of rate table rotation 180 °/s, c) close-loop controlled thermal ovenization.

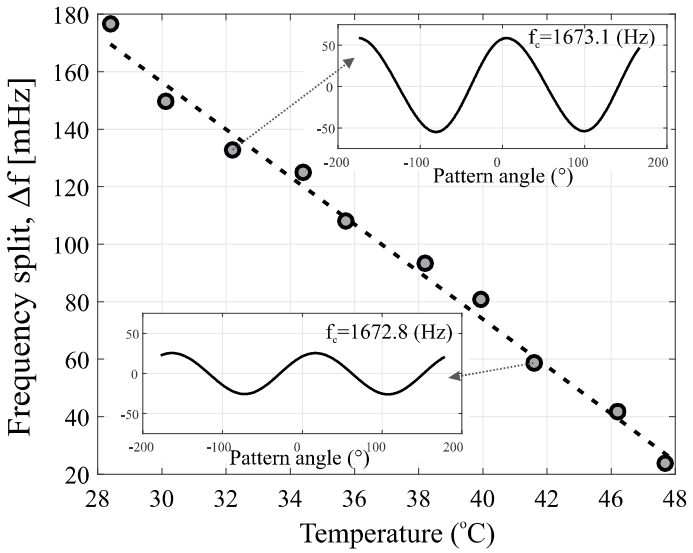

Fig. 7. Experimental characterization of the frequency split vs. temperatures set by TEC through virtual carouseling. Inset figures: two examples of virtual carouseling of the gyroscope at 30°C and 37°C temperatures observing changes in frequency split and shift in the drive center frequency (f_c).

variations in frequency mismatch Δf over 20°C temperature change. The phenomenon was only observed experimentally on this particular high quality factor device. We expect the trend will be different through different samples.

To observe the effect of temperature on the angular gain, the gyro was operated in the WA mode. A constant angular rate of 180 °/s (well above the minimum detectable angle for this device) was applied to the rate table and the angular gain was calculated at different temperatures set by the thermal controller. The angular gain as a function of temperature of the LCC package is plotted in Fig. 8. Each measurement point represents an average of roughly 100s of continuous rotation. In the WA mode, at a given temperature T, the frequency mismatch can be calculated from the fluctuation range of the VCO frequency output (similar to VC). The frequency mismatch extracted in the WA mode matches closely the frequency mismatches measured by the VC operation. The results demonstrate a strong correlation between the angular gain drift and the temperature-induced frequency mismatch. The exact trend of frequency mismatches might be unique to the studied sample.

IV. Correction Algorithm

The drift in the angular gain was corrected by the least-squares linear fit between the measured dependence of the frequency mismatch and the temperature. An algorithm was implemented to correct the drift by sensing of the frequency mismatch variation. Two examples are provided to show fluctuations of the frequency mismatch during experiments: 1) applied rotation in a closed environment inside a high speed centrifuge system to observe a baseline angular gain drift, and 2) elevation of the LCC package temperature during rotation with applied retrospective correction.

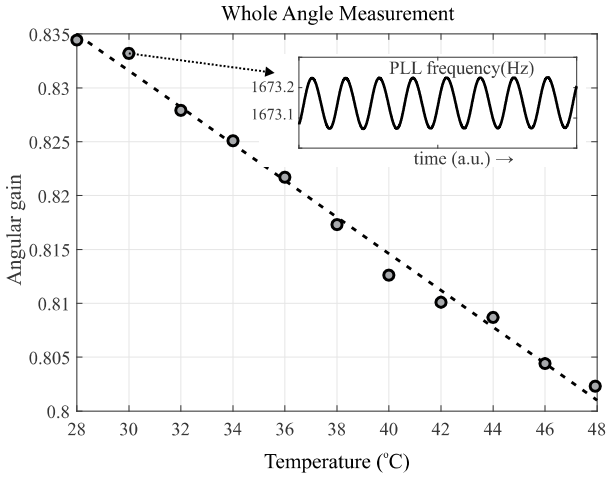

Fig. 8. Experimentally extracted angular gain under different temperatures in WA mode, illustrates 4% deviation of angular gain over 20°C temperature change. The figure inset shows an example of the corresponding frequency of the PLL control over time at a fixed 30°C temperature

The input rate rotation of $180°/s$ was applied to the rate table. The WA mode algorithms were enabled when the temperature of the electronics reached a plateau, to eliminate changes observed earlier (section III). Fig. 9 shows the extracted frequency tracking from the PLL loop under continuous rotation without thermal control (Example 1). The result suggested a shift of 1.5mHz for 400s as a baseline angular gain drift. Fig. 10 demonstrates experimentally the measured angular gain drift for an accumulated input rotation of 1.8×10^5 deg (Example 2). An external temperature cycle was applied to the device during the WA operation using the closed loop thermal stage. The frequency mismatch was calculated using the recorded VCO, an output from the PLL loop. The correction was made by the identified virtual carouseling coefficients between frequency mismatch and angular gain by a look-up table. The 2.2% drift of the angular gain was corrected in post-processing and shown in Fig. 10.

Conclusion

We experimentally demonstrated the effect of quadrature and thermal variations on the angular gain drift of a MEMS

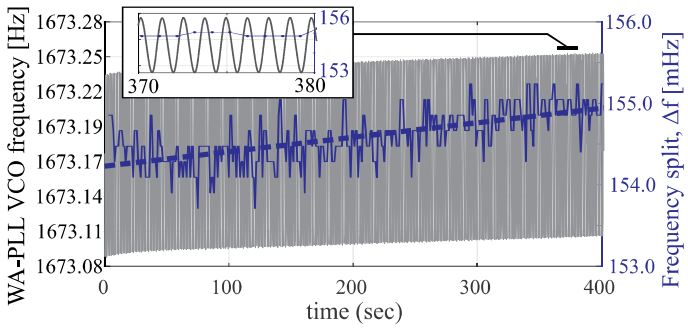

Fig. 9. Experimental tracking of PLL's VCO frequency in the WA mode of operation. The inset figure demonstrate the periodic function of the standing wave frequency. The frequency mismatch was estimated over a sliding 3s window with the step of 1s.

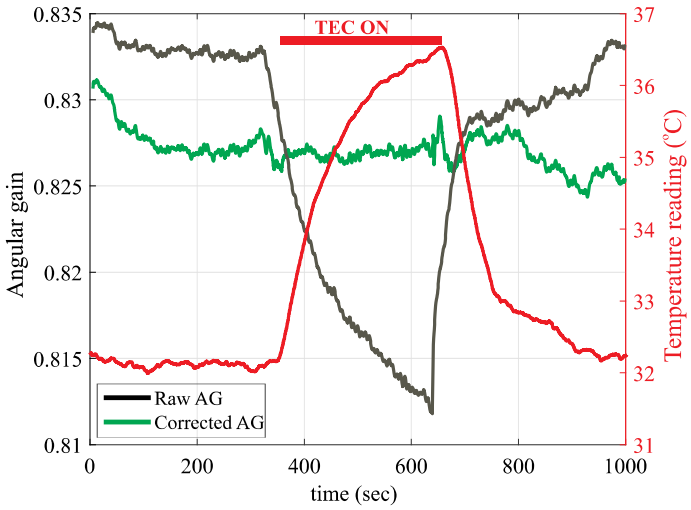

Fig. 10. Deviation of gyroscope angle output over 10000s without temperature control (black). Correction of the angular gain drift demonstrates a scale factor improvement of direct measurements of the angle from precession (green).

gyroscope operating in the whole angle mode and proposed an identification and compensation algorithm. The effect of frequency mismatch variations on the angular gain drift in a non-ideal high-Q gyroscope was correlated to the temperature fluctuations. The frequency mismatch variations were identified by virtual carouseling and used as an input to the feed-forward correction algorithm to compensate for the angular gain drift in the WA mode.

References

[1] S. Askari, M. H. Asadian, and A. M. Shkel, "High quality factor MEMS gyroscope with whole angle mode of operation," in *IEEE INERTIAL, Lake Como, Italy*, March 2018, pp. 1–4.

[2] D. D. Lynch, "Vibratory gyro analysis by the method of averaging," in *The 2nd St. Petersburg Int. Conf. on Gyroscopic Technology and Navigation, Saint Petersburg, Russia*, May 1995.

[3] I. P. Prikhodko, J. A. Gregory, and M. W. Judy, "Virtually rotated MEMS gyroscope with angle output," in *IEEE 30th International Conference on Micro Electro Mechanical Systems (MEMS), Las Vegas, NV, USA*, Jan 2017, pp. 323–326.

[4] G. Remillieux and F. Delhaye, "Sagem Coriolis Vibrating Gyros: A vision realized," in *DGON Inertial Sensors and Systems (ISS) Symposium, Karlsruhe, Germany*, 2014, pp. 1–13.

[5] A. A. Trusov *et al.*, "Non-axisymmetric Coriolis Vibratory Gyroscope with Whole Angle, Force Rebalance, and Self-calibration," in *Solid-State Sensors, Actuators, and Microsystems Workshop, Hilton Head Island, SC, USA*, June 2014, pp. 419–422.

[6] A. A. Trusov *et al.*, "mHRG: Miniature CVG with beyond navigation grade performance and real time self-calibration," in *IEEE INERTIAL, Laguna Beach, CA, USA*, Feb 2016, pp. 29–32.

[7] D. Senkal, A. Efimovskaya, and A. M. Shkel, "Minimal realization of dynamically balanced lumped mass WA gyroscope: Dual Foucault Pendulum," in *IEEE International Symposium on Inertial Sensors and Systems, Hapuna Beach, HI, USA*, March 2015, pp. 1–2.

[8] P. Taheri-Tehrani, A. D. Challoner, and D. A. Horsley, "Micromechanical rate integrating gyroscope with angle-dependent bias compensation using a self-precession method," *IEEE Sensors Journal*, vol. 18, no. 9, pp. 3533–3543, May 2018.

[9] D. M. Rozelle, "The hemispherical resonator gyro: From wineglass to the planets," in *Proc. 19th AAS/AIAA Space Flight Mechanics Meeting, Savannah, Georgia, USA*, 2009, pp. 1157–1178.

[10] R. L. Kubena, R. J. Joyce, and A. D. Challoner, "Correlation of frequency, temperature, and bias stability of a Si ring gyro," in *IEEE INERTIAL, Laguna Beach, CA, USA*, Feb 2016, pp. 21–24.